A LBNL-4695E

Airflow Simulations around OA Intake Louver with Electronic Velocity Sensors

Hwataik Han[1], Douglas P. Sullivan[2] and William J. Fisk[2]

[1]Kookmin University
Seoul, South Korea

[2]Environmental Energy Technologies Division
Indoor Environment Department
Lawrence Berkeley National Laboratory
Berkeley, CA

April 2009

This work was supported by Kookmin University and National Research Foundation of Korea Grant funded by the Korean Government (09-0260). The experiments were supported by the California Energy Commission through the San Diego State University Research Foundation under contract 54915A/06-03B through Contract No. DE-AC02-05CH11231 between the University of California and the U.S. Department of Energy.

Airflow Simulations around OA Intake Louver with Electronic Velocity Sensors

Hwataik Han*[1], Douglas P. Sullivan[2] and William J. Fisk[3]

[1] Professor, Kookmin University, Korea
[2] Research Associate, Indoor Environment Department, Lawrence Berkeley National Laboratory, USA
[3] Director, Indoor Environment Department, Lawrence Berkeley National Laboratory, USA

Abstract

It is important to control outdoor airflow rates into HVAC systems in terms of energy conservation and healthy indoor environment. Technologies are being developed to measure outdoor air (OA) flow rates through OA intake louvers on a real time basis. The purpose of this paper is to investigate the airflow characteristics through an OA intake louver numerically in order to provide suggestions for sensor installations. Airflow patterns are simulated with and without electronic air velocity sensors within cylindrical probes installed between louver blades or at the downstream face of the louver. Numerical results show quite good agreements with experimental data, and provide insights regarding measurement system design. The simulations indicate that velocity profiles are more spatially uniform at the louver outlet relative to between louver blades, that pressure drops imposed by the sensor bars are smaller with sensor bars at the louver outlet, and that placement of the sensor bars between louver blades substantially increases air velocities inside the louver. These findings suggest there is an advantage to placing the sensor bars at the louver outlet face.

Keywords: ventilation; outdoor air louver; computational fluid dynamics; velocity sensor installation

1. Introduction

The amount of outdoor air ventilation provided to buildings influences building energy consumption and can affect the health and work performance of the occupants of the building (Seppanen and Fisk 2004). Despite the importance of ventilation, in multi-building surveys of commercial buildings the measured ventilation rates are often well above or below the rates specified in ventilation codes (ANSI/ASHRAE 2004) and standards (Fisk *et al.* 2005b); i.e., ventilation rates are often poorly controlled. Systems for real time or periodic measurement of rates of outdoor air flow into HVAC systems, integrated with suitable controls (Kwon and Han 2007), could enable better control of building ventilation rates. The outdoor air generally enters HVAC systems through OA intake louvers that have complicated geometries designed to limit moisture entry. The geometry of the louvers, and the low air speeds maintained in louvers, lead to low and spatially uneven air velocities downstream of louvers that make it difficult to accurately measure the outdoor air flow rates (Fisk *et al.* 2005b). Often, there is no section of straight ductwork in the outdoor airstream to facilitate measurements. The results of prior experimental research suggest that placement of velocity sensors between louver blades or directly adjacent to the louver outlet may be advantageous relative to the more common practice of placing velocity sensors some distance downstream of the louver (Fisk *et al.* 2005a). The louver largely controls the velocity profile inside the louver or at the outlet face of the louver – and a repeatable velocity profile facilitates accurate measurements of flow rates. The louver also increases the air speed, relative to the downstream speed, which also facilitates accurate measurements with most velocity sensors. Experimental studies (Fisk *et al.* 2008) are underway at Lawrence Berkeley National Laboratory to evaluate measurement of outdoor air flow rates using electronic velocity sensors installed between louver blades or installed directly adjacent to the outlet plane of louvers. This paper, describes the use of numerical modeling, for one type of louver, to provide further insight into the design and performance of these measurement systems.

*Contact Author: Hwataik Han, Professor, Kookmin University, 861-1 Jeungneung-dong, Seongbuk-gu, Seoul 136-702, Korea
Tel: +82-2-910-4687 Fax: +82-2-910-4839
E-mail: hhan@kookmin.ac.kr
(Received April 7, 2009 ; accepted February 5, 2010)

2. Numerical Analysis

2.1 Numerical Model

The calculation domain is shown in Fig.1., which has the dimensions of 1.8m x 1.8m x 1.8m. A louver, Model Arrow EA64 is located in the middle of the calculation domain, facing in the horizontal direction.

The nominal intake area of the louver is 0.6m x 0.6m. Details of the louver configurations are shown in Fig.2. and Fig.3. There are four horizontal openings through the louver. The configurations of louver outlet and inlet face are slightly different from each other. Fig.3. also shows two sets of sensor locations, i.e. middle of blades (Cross-section 1) and downstream of blades (Cross-section 2). Bird screens are neglected in all cases.

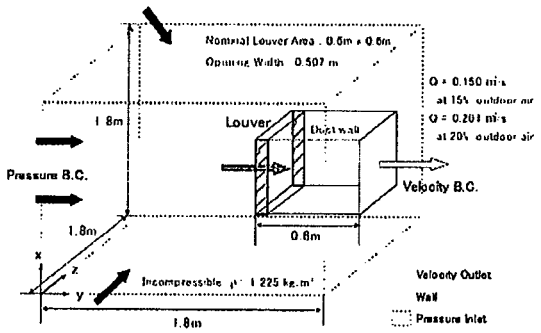

Fig.1. CFD Calculation Domain

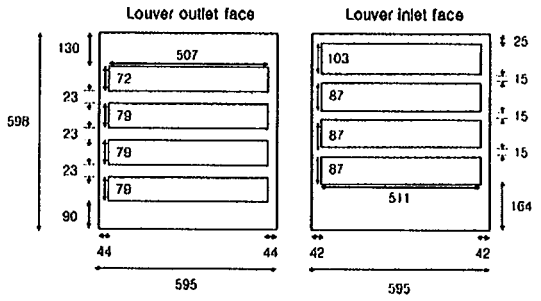

Fig.2. Opening Areas of the Louver with Dimensions in mm

As the sensor configurations (Ebtron 2009) are complicated, they are simplified for modeling as is shown in Fig.4. A hole through the sensor bar is represented as a cut-off gap between two cylindrical bars. The gap distance is chosen as a hydraulic diameter of the hole diameter and the bar diameter. The velocity profiles will be shown at two cross-sections, i.e. crossing the middle of the gap between bars (cross-section A) and crossing the middle of the bar (cross-section B). The cross-section B would provide the airflow simulation around the sensor bar, and the cross-section A would indicate the velocity magnitude measured by the sensor.

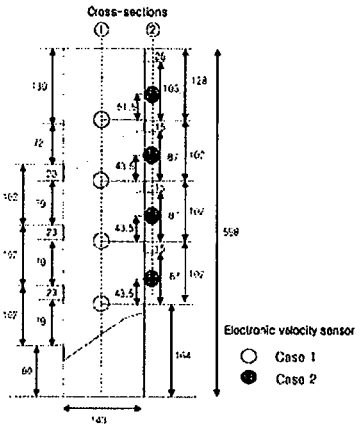

Fig.3. Details of Louver Vanes and Sensor Locations with Dimensions in mm

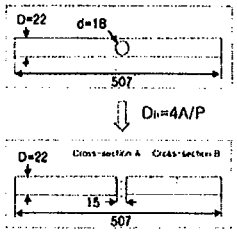

Fig.4. Geometry of a Velocity Probe with Actual Opening for a Velocity Sensor (Top) and with Simplified Geometry Used in Modeling with Dimensions in mm

2.2 Simulation Procedure

A commercial CFD package (ANSYS 2009) has been used to simulate turbulent airflows in the calculation domain. The governing equations are the time-averaged Navier-Stokes equation:

$$div(\rho V \Phi - \Gamma_\Phi \, grad\, \Phi) = S_\Phi \qquad (1)$$

where Φ is one of the variables to solve as are shown in Table 1., and S_Φ and Γ_Φ are the source term and the diffusion coefficient for the variable. ρ is the air density, and V is the velocity vector. The fluid is assumed to be incompressible and Newtonian in behavior with negligible buoyancy and viscous dissipation.

Table 1. Variables and Coefficients for the Governing Equation

Equation	Variable (Φ)	Diffusion coefficient (Γ_Φ)	Source term (S_Φ)
Continuity	1	0	0
Momentum	V_i	$\mu+\mu_t$	$-\partial P/\partial x_i$
Turbulent kinetic energy	k	$(\mu+\mu_t)/\sigma_k$	$P_k-\rho\varepsilon+G_k$
Turbulent kinetic energy dissipation rate	ε	$(\mu+\mu_t)/\sigma_\varepsilon$	$\varepsilon(C_1P_k-C_2\rho\varepsilon)/k+C_3G_k\varepsilon/k$

$P_k=\mu_t(V_{i,j}+V_{j,i})V_{i,j}$, $\mu_t=C_\mu\rho k^2/\varepsilon$, $(\sigma_k,\sigma_\varepsilon,C_1,C_2,C_3,C_\mu)=(1.0,1.314,1.44,1.92,1.0,0.09)$

The standard k-ε model (Launder and Spalding, 1974) has been used for turbulence modeling. The diffusion coefficients and source term expressions are shown in Table 1.

Boundary conditions are treated differently for inlet, outlet, and wall surfaces. Velocity boundary conditions are given for the duct outlet according to the specified airflow rates, and pressure boundary conditions are given for far-field inlet surfaces except the sidewall around the duct outlet. The far-field boundaries are treated as free boundaries. The gradients of both the normal and tangential velocities are given zero. Turbulence kinetic energy and its dissipation rate are also considered to be zero at the boundaries. No slip conditions are given on all wall surfaces including louver blades and duct surfaces. The standard log-wall functions of Launder and Spalding are adopted for the grid points next to the wall surface.

The basic algorithm for solving the governing equations is the SIMPLE algorithm by Patankar (1980). The number of meshes is approximately 76000. The thickness of blade vane is neglected. The convergence criteria have been chosen as 10^{-7}. The number of iterations ranges between 800 and 1000, and the calculation time ranges between 1.5 to 2 hours for each run. Simulations have been conducted for two airflow rates, 0.150 m^3/s (318 CFM, 15% of maximum recommended flow through louver) and 0.201 m^3/s (425 CFM, 20% of maximum recommended flow through louver).

3. Results

3.1 Airflow in Louver without Sensors

The overall flow patterns are shown in Fig.5. for the airflow rate of 0.15 m^3/s when velocity sensors are not installed. Color indicates velocity magnitude. It can be observed that air is entrained from the surroundings. The calculation domain is large enough so that the airflow pattern inside the duct is believed not to be influenced significantly by the far-field boundary conditions. The air entrained through the louver creates a large recirculation eddy in the duct because of the angle of the louver blades and the blocking of the duct perimeter by the frame of the louver. The existence of this eddy was also evident when smoke was used to show airflow profiles. There are small eddies behind the backward steps of louver blades.

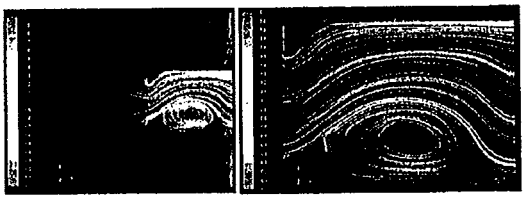

Fig.5. Flow Patterns in Calculation Domain and Inside Duct Behind Louver (0.15 m^3/s). The Air Flows from Left to Right

The flow patterns for the airflow rate of 0.20 m^3/s are not illustrated here, but are similar to Fig.5. These numerical predictions are quite consistent with the airflow patterns visualized using smoke injections in the previous experiments (Fisk *et al.* 2008).

Fig.6. shows the velocity magnitude profiles along the x-axis in the middle of blades and downstream of blades. There are four peaks appearing in the plot, since there are four openings for the louver tested in the present study. The first bump corresponds to the velocity profile through the bottom-most opening (opening 1). The velocity maximum occurs in the middle of each opening, but not at the exact center. The volumetric airflow rate for each passage is related to but is not the same as the area under the corresponding curve, since the velocity is not perpendicular to the x-z plane. At the exit surface (cross-section 2), the velocity is not zero below x=0.764m where the first opening starts, since the cross-section 2 is away from the exit surface by the half-thickness of the sensor bars.

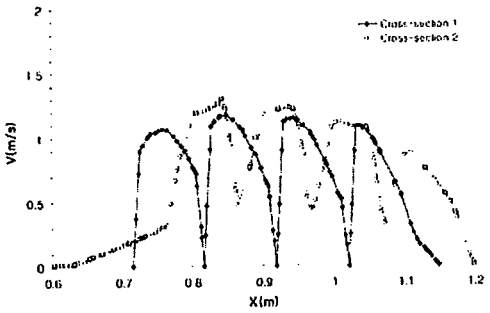

Fig.6. Velocity Plots Between Blades (Cross-sections 1) and Downstream of Blades (Cross-section 2) with No Sensors Installed (Q=0.15 m^3/s)

3.2 Airflow with Sensors installed

Velocity magnitude distributions can be seen in contour plots, as in Fig.7. for Case 1 with sensors mounted between blades. Fig.7a. and 7b. are the flow patterns at the cross-section of A and B, respectively.

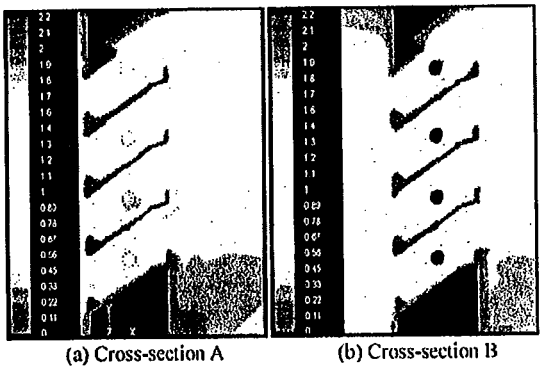

(a) Cross-section A (b) Cross-section B

Fig.7. Two-dimensional Plots of Velocity Magnitude with Sensors between Blades (Case 1, 0.15 m^3/s)

The cross-sections of circular sensor bars are shown in Fig.7b., but are added with dotted lines in Fig.7a. It seems the velocity magnitude is greater inside dotted circles in Fig.7a. (shown in red) than that around the circles. In Fig.7b., the velocity is zero inside circles (shown in black) which represent the cross section of the cylinder of the sensor bars and air flows around the cylindrical bars. Velocity magnitudes are small near louver blades and walls (shown in blue) and show complicated distributions between blades.

Velocity magnitudes are plotted between blades in Fig.8. along the centerlines of the cross-sections A and B. The dotted line indicates the case without sensors mounted. The maximum velocity is the largest in the second opening, and the smallest in the top-most one. The velocity profiles are changed when the sensor bars are mounted between blades. The velocities are greatly increased by inserting sensor bars since the passage areas are decreased by the amount of the cross-sectional area of the sensors. The velocity magnitudes measured with air velocity sensors are superimposed in the figure. They show quite good agreements with the numerical data with the passage blocked by the sensors.

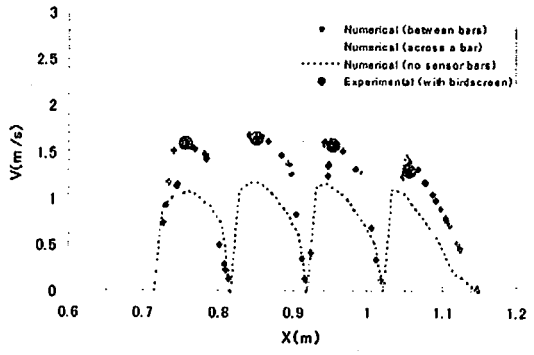

Fig.8. Velocity Magnitude between Blades with Sensors Mounted for Case 1 (Q=0.15 m^3/s)

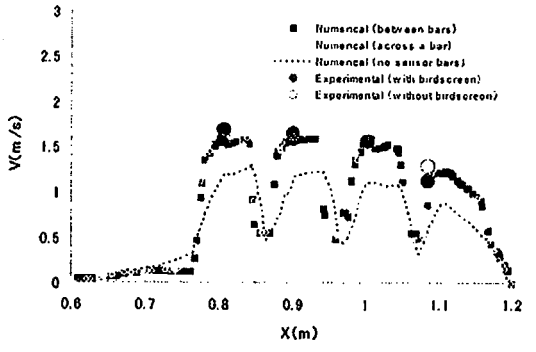

Fig.9. Velocity Magnitude Downstream of Blades with Sensors Mounted for Case 2 (Q=0.15 m^3/s)

Fig.9. shows the velocity profiles for Case 2 at the downstream face of the louver blades. The velocity profiles are similar but slightly flatter between blades compared to Fig.8., since there are open areas around the sensors at the end of the louver blades. Similar discussions are possible for this case also. There are two sets of experimental data superimposed in the figure, i.e. one with a bird screen and the other without a bird screen positioned at the louver outlet. Previous experiments have indicated that the presence of a bird screen does not significantly affect the velocity measurements.

Figs.10. and 11. are the velocity profiles for the flow rate of 0.20 m^3/s for Case 1 and Case 2, which correspond to Figs. 8 and 9 for 0.15 m^3/s. Further discussions are not included here, since the profiles are similar except that the magnitudes increased by the factor of 1.33, approximately.

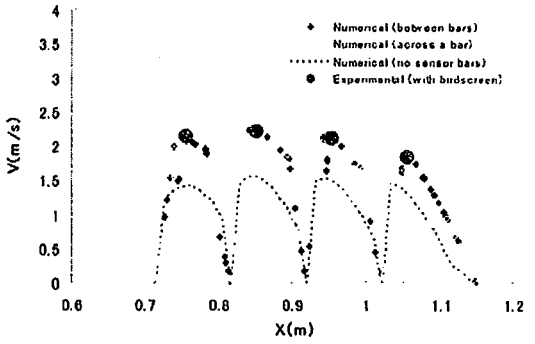

Fig.10. Velocity Magnitude between Blades (Case 1) with and without Sensors Mounted (Q=0.20 m^3/s)

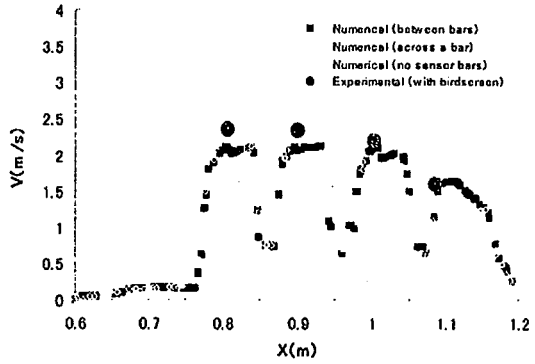

Fig.11. Velocity Magnitude Downstream of Blades (Case 2) with and without Sensors Mounted (Q=0.20 m^3/s)

3.3 Effect of Sensor Bars on Velocity Maximums

The velocity maximums through the openings are shown in Table 2. along with their averages and standard deviations. The averages of the four maximums of Case 1 are slightly greater than those of Case 2 for both airflow rates of 0.15 and 0.20 m^3/s. The

Table 2. Velocity Maximums through the Openings. Numbers in Parenthesis Indicate the Measured Values. (Fisk *et al.* 2008)

Flow	Q=0.15 m^3/s		Q=0.20 m^3/s	
Blades	Middle (Case 1)	Down stream (Case 2)	Middle (Case 1)	Down stream (Case 2)
Opening 1	1.57 (1.59)	1.58 (1.69)	2.07 (2.15)	2.11 (2.36)
Opening 2	1.68 (1.64)	1.59 (1.65)	2.23 (2.22)	2.12 (2.34)
Opening 3	1.63 (1.57)	1.58 (1.57)	2.15 (2.11)	2.11 (2.20)
Opening 4	1.44 (1.29)	1.23 (1.14)	1.90 (1.84)	1.63 (1.59)
Average	1.58 (1.52)	1.50 (1.51)	2.09 (2.08)	1.99 (2.12)
Standard deviation	0.10 (0.16)	0.18 (0.25)	0.14 (0.17)	0.24 (0.36)

standard deviations of Case 1 are lower than those of Case 2 for both the airflow conditions.

The velocities through the openings are quite uniform except the fourth one. The experimental results also indicate that the velocity magnitudes are the lowest for the fourth opening. The overall airflow rate through a louver would be affected by ways of averaging individual velocities, since the opening area and airflow patterns are different from each other.

3.4 Effect on Airflow Ratios through Openings

The airflow through each opening can be calculated by integrating velocity over the entire incoming area. Estimates of the airflow rates at a cross-section are shown in Fig.12. for Q=0.15 m^3/s and in Fig.13. for Q=0.20 m^3/s. Opening 1 indicates the bottom-most passage between adjacent louver blades, and the opening 4 indicates the top-most passage. The figures show relative airflow rates through openings for different cases. The openings 2 and 3 show greater airflow rates than the openings 1 and 4. The relative airflow rates are also affected by the sensor locations.

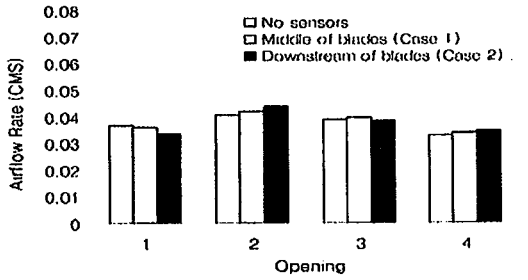

Fig.12. Relative Airflow Rates through Openings (0.15 m^3/s)

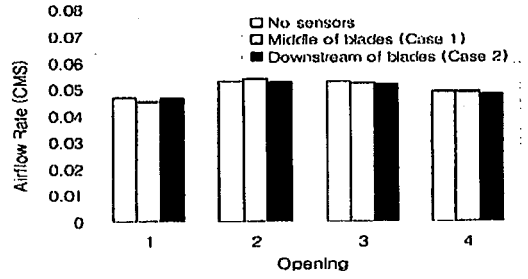

Fig.13. Relative Airflow Rates through Openings (0.20 m^3/s)

The standard deviation of the airflow rates for Case 1 is slightly lower than that for Case 2 at Q=0.15 m^3/s, but vice versa at Q=0.20 m^3/s. The relative airflow rates through openings are somewhat different from the relative velocities shown in Table 2. because of the area differences.

3.5 Effect of Sensor Bars on Overall Pressure Drop

The pressure drops generated by the sensors are listed in Table 3. The pressure indicates the pressure in the middle of the exit. The overall predicted pressure drop by the louver is itself 1.94 Pa which compares to an estimated 1.2 Pa by extrapolation from the louver manufacturer's data. The predicted pressure drops with the sensors installed for Case 1 and 2 are 3.56 Pa and 2.89 Pa respectively for the airflow rate of 0.15 m^3/s. The sensors in the middle of the blades create slightly larger pressure drop compared to those at the downstream of the blades, as can be expected. The predicted pressure drops for 0.20 m^3/s are 3.42, 6.15, and 5.04 Pa respectively. It can be seen that pressure drop is nearly proportional to the square of the airflow rate for the same configurations, i.e. $(0.20/0.15)^2=1.78$ times.

Table 3. Pressure Losses through Louver with Sensors

Sensor location	Q=0.15 m^3/s	Q=0.20 m^3/s
No sensors	1.94	3.42
Middle of blades (Case 1)	3.56	6.15
Downstream of blades (Case 2)	2.89	5.04

4. Discussions

The numerical simulations provide some insight with respect to measurement system design. The numerical results do not point to any substantial barriers to these investigated measurement approaches. A comparison of Figs.10. and 11. indicates that the velocities at the louver outlet are more uniform (i.e., the profile is flatter) relative to velocities between louver blades. These results suggest that a highly precise placement of the velocity sensors will be less important if the sensors are at the louver outlet face. The predicted pressure drops are slightly lower with the sensors located at the louver outlet – another small advantage to installing probes at this location, although the overall pressure drops are small enough to be of only modest concern. The good agreement of predictions with experimental data suggest that numerical modeling might enable calibration equations to be developed for louver-sensor configurations without laboratory testing, although substantial additional model-measurement comparisons would first be necessary.

5. Conclusions

The CFD simulations yielded velocity magnitudes in good agreement with experimental data and confirmed the experimental observation of a large eddy located downstream of the louver. The CFD modeling identified no barriers to these approaches for measuring OA flow rates. The detailed information provided

by the CFD simulations provided insights regarding measurement system design. The simulations indicated that velocity profiles are flatter (more spatially uniform) at the louver outlet relative to between louver blades, that pressure drops imposed by the sensor bars are smaller with sensor bars at the louver outlet, that placement of the sensor bars between louver blades substantially increases air velocities inside the louver, and that velocities vary moderately among the different airflow passages of the louver. The first three of these findings suggest that there is a slight advantage to placing the sensor bars at the louver outlet face. Flatter velocity profiles at the louver outlet make precise sensor placement less critical. The lower pressure drops with sensor bars at the louver outlet are preferable from an energy perspective. Also, the lower velocities inside the louver when the sensor bars are installed at the louver outlet may improve the moisture removal performance of the louver. The fourth finding indicates the advantage of using multiple velocity sensors distributed relatively uniformly at the louver outlet face or within the louver.

Acknowledgements

This work was supported by Kookmin University and National Research Foundation of Korea Grant funded by the Korean Government (09-0260). The experiments were supported by the California Energy Commission through the San Diego State University Research Foundation under contract 54915A/06-03B through Contract No. DE-AC02-05CH11231 between the University of California and the U.S. Department of Energy.

References

1) ANSI/ASHRAE (2004) Ventilation for Acceptable Indoor Air Quality. ASHRAE Standard 62-1. Atlanta. American Society of Heating, Refrigerating, and Air-Conditioning Engineers.
2) Ebtron (2009) Master Product Catalog. Ebtron, p.28.
3) ANSYS (2009) Fluent 6.2 User Guide.
4) Fisk, W.J., Faulkner, D., and Sullivan, D.P. (2005) Technologies for measuring flow rates of outdoor air into HVAC systems: some causes and suggested cures for measurement errors. ASHRAE Transactions 2005a, 111(2), pp.456-463.
5) Fisk, W.J., Faulkner, D., and Sullivan, D.P. (2005) An evaluation of three commercially available technologies for real-time measurement of rates of outdoor airflow into HVAC systems. ASHRAE Transactions 2005b, 111(2), pp.443-455.
6) Fisk, W.J., Sullivan, D.P., Cohen, S., and Han, H. (2008) Measuring outdoor air intake rates using electronic velocity sensors at louvers and downstream of airflow straighteners. Lawrence Berkeley National Laboratory Report, LBNL-1250E, Berkeley, CA.
7) Kwon, Y.I. and Han, H. (2007) A study on the evaluation of air change efficiency of multi-air-conditioner coupled with ventilation system. Int J of Air-Conditioning and Refrigeration, 15(3), pp.101-107.
8) Launder, B.E. and Spalding, D.B. (1974) The numerical computation of turbulence flows. Computer Methods in Applied Mechanics and Engineering, 3, pp.269-289.
9) Patankar, S.V. (1980) Numerical heat transfer and fluid flow. Washington: Hemisphere Publishing.
10) Seppanen, O. and Fisk, W.J. (2004) Summary of human responses to ventilation. Indoor Air, 14 (supplement 7), pp.102-118.